ACS Catalysis

Research Article

pubs.acs.org/acscatalysis

Bifunctional Catalytic System Effective for Oxidative Dehydrogenation of 1-Butene and *n*-Butane Using Pd-Based Intermetallic Compounds

Shinya Furukawa,[†] Masahiro Endo,[‡] and Takayuki Komatsu*[,‡]

[†]Department of Chemistry, [‡]Department of Chemistry and Materials Science, Tokyo Institute of Technology, 2-12-1-E1-10 Ookayama, Meguro-ku, Tokyo 152-8551, Japan

Supporting Information

ABSTRACT: The catalytic performance of Pd-based intermetallic compounds supported on silica (Pd_mM_n/SiO_2: M = Bi, Fe, Ge, In, Sn, Zn) was investigated in oxidative dehydrogenation of 1-butene and *n*-butane. A remarkable increase in selectivity (and also yield) of dehydrogenation products (1,3-butadiene and/or 1-butene) was obtained when PdIn, PdBi, or Pd_3Fe replaced monometallic Pd. Temperature-programmed reduction and X-ray diffraction (XRD) studies on the catalysts with various treatments (i.e., the fresh, spent, and calcined) suggested that redox of the second metal was involved in the catalysis. XRD, X-ray photoelectron spectra, and transmission electron microscopy−energy dispersive X-ray spectroscopy analyses using the spent $PdIn/SiO_2$ catalyst revealed the formation of a core−shell structure consisting of a $PdIn_{1-\delta}$ core and Pd−In_2O_3 composite shell formed by oxidative decomposition of PdIn during the reaction. A mechanistic study suggested that the presence of In atoms, adjacent to Pd atoms, effectively inhibits the undesired combustion by capturing O_2 as lattice oxygen. The incorporated lattice oxygen reacts with hydrogen atoms derived from the hydrocarbon by C−H activation over Pd sites, resulting in the formation of water and oxygen vacancy and/or the parent intermetallic phase. We thus reveal that a combination of C−H activation by Pd and the redox of the second metal provides a unique and effective dehydrogenation system.

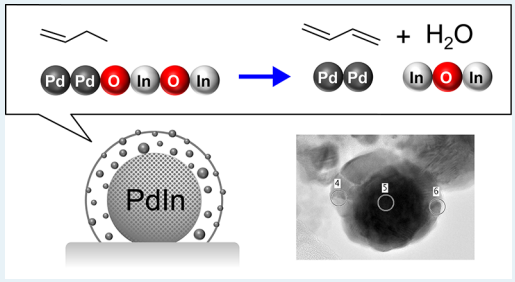

KEYWORDS: *oxidative dehydrogenation, butadiene, intermetallic compound, bifunctional, 1-butene*

INTRODUCTION

1,3-Butadiene is an important feedstock of butadiene polymer, the demand for which is expanding.[1] In general, it is produced by dehydrogenation of 1-butene.[2] The dehydrogenation process is divided into two categories: (1) nonoxidative and (2) oxidative dehydrogenation,[3] as described in the following equations.

$$C_4H_8 \rightarrow C_4H_6 + H_2 \qquad \Delta H^\circ = 110\text{kJ}\cdot\text{mol}^{-1} \tag{1}$$

$$C_4H_8 + 1/2\ O_2 \rightarrow C_4H_6 + H_2O \qquad \Delta H^\circ = -132\text{kJ}\cdot\text{mol}^{-1} \tag{2}$$

The nonoxidative process is highly endothermic, requiring high temperatures to obtain a reasonable conversion. In addition, the deposition of coke should be suppressed in order to maintain the catalytic performance. In this context, oxidative dehydrogenation possesses attractive advantages. The reaction is exothermic with no limitation by equilibrium; therefore, it is essentially possible to obtain a complete conversion at low temperatures. Moreover, deposited coke can be removed by oxidation into CO_x.

Oxidative dehydrogenation of hydrocarbons has been widely investigated using metal oxide catalysts.[4−11] Among a number of oxide catalysts, bismuth molybdates are widely investigated and known to be effective for the oxidative dehydrogenation of 1-butene to 1,3-butadiene.[4−7] On the other hand, very few researchers have studied oxidative dehydrogenation of hydrocarbons using noble metal catalysts,[12,13] despite possessing greater C−H activation abilities than transition metal oxides, which is extremely important in the dehydrogenation process. This may be a product of the highly active properties of noble metals causing undesired combustion of hydrocarbons into CO_x, significantly decreasing selectivity. In this context, the development of an effective catalyst based on the use of a noble metal for oxidative dehydrogenation would open up a new field of catalytic dehydrogenation. It is an ideal approach to modify the nature of the metallic catalysts so that combustion is suppressed without lowering their C−H activation ability. One can modify the nature of metallic catalysts by changing catalyst support, adding cocatalysts, and by the formation of an alloy or intermetallic phase. We previously reported that some intermetallic catalysts exhibited superior catalytic performances for the nonoxidative dehydrogenation of hydrocarbons than monometallic catalysts, for example, Ni_3Sn/SiO_2 and Ni_3Sn_2

Received: June 28, 2014
Revised: September 1, 2014
Published: September 2, 2014

   dx.doi.org/10.1021/cs500920p | ACS Catal. 2014, 4, 3533−3542

showed higher selectivities than Ni/SiO_2 in the dehydrogenation of cyclohexane to benzene.[14] Pt_3Sn/SiO_2 exhibited not only higher selectivity but also greater catalytic activity than Pt/SiO_2 in *n*-butane dehydrogenation to butenes.[15] Although this Pt-based catalyst showed high catalytic performance in dehydrogenation of *n*-butane, the high oxidizing ability of Pt may result in a larger amount of combustion to CO_x in the oxidative dehydrogenation condition. Therefore, we focused on Pd-based intermetallic compounds as candidates of effective catalysts for oxidative dehydrogenation of 1-butene.

In this study, we investigated the catalytic properties of various Pd-based intermetallic compounds supported on SiO_2 (Pd_mM_n/SiO_2: M = Bi, Fe, Ge, In, Sn, Zn) in the oxidative dehydrogenation of 1-butene, for the formation of 1,3-butadiene. Dehydrogenation of *n*-butane to 1-butene and 1,3-butadiene was also examined using the Pd-based catalysts. A mechanistic study and detailed characterizations were performed to understand the catalysis of intermetallic compounds.

Herein, we report the development of catalysts superior to monometallic Pd and unique bifunctional catalysis played by Pd and the second metal.

EXPERIMENTAL SECTION

Catalyst Preparation. Monometallic Pd/SiO_2 was prepared by pore-filling impregnation. An aqueous solution of $Pd(NO_3)_2$ (4.8×10^{-2} g·mL^{-1}, 0.64 mL, N.E. ChemCat) was diluted with ion-exchanged water and added to silica gel (5.0 g, Cariact G-6, Fuji Silysia Co., S_{BET} = 673 m^2·g^{-1}) previously dried at 130 °C and cooled in air to room temperature. The quantity of palladium solution was calculated to fill the silica gel pores, achieving a palladium loading of 3 wt %. The mixture was sealed with plastic film overnight at room temperature. It was then dried over a boiling water bath with stirring, followed by drying at 130 °C for 1 h, and subsequently calcined in the air at 400 °C for 1 h. After the calcination, the catalyst was reduced under flowing hydrogen (99.9995%, 60 mL·min^{-1}; Taiyo Nippon Sanso) at 400 °C for 2 h. The catalyst was cooled to room temperature with flowing helium and kept in a desiccator. Pd/In_2O_3 was prepared in a similar way using In_2O_3 (99%, Wako) as a support. Pd-based intermetallic compound catalysts (Pd_mM_n/SiO_2; M = Ge, In, Sn, Zn) were prepared by successive impregnation with Pd/SiO_2. In the case of Pd−Zn (1:1), an aqueous solution of $Zn(NO_3)_2{\cdot}6H_2O$ (99%, Kanto) was added to Pd/SiO_2 so that the atomic ratio of Pd/Zn was adjusted to 1. The mixture was sealed using plastic film and left overnight at room temperature. It was then dried over a boiling water bath with stirring and reduced under flowing hydrogen (99.9995%, Taiyo Nippon Sanso) at 800 °C 2 h. Other intermetallic catalysts were prepared in a similar way using specific second metal precursors, solvents, and reduction temperatures: PdIn, In(acetylacetonate)$_3$ (95%, Kanto), nitric acid (60%, Kanto), 400 °C; Pd_2Ge, tetrabutylgermane (98%, Aldrich), *n*-hexane (, 99%, Kanto), 700 °C; Pd_3Sn_2, $SnCl_2{\cdot}2H_2O$ (98%, Kanto), H_2O/MeOH (1:1), 600 °C. $PdBi/SiO_2$ was prepared by coimpregnation in a mixed nitric acid solution of $Pd(NO_3)_3$ and $Bi(NO_3)_3$ and reduced under H_2 at 500 °C for 1 h. Pd_3Fe/SiO_2 was also prepared by coimpregnation in a similar manner to $PdBi/SiO_2$ using Fe(acetylacetonate)$_3$ (99%, Soekawa) at an 800 °C reduction temperature. In_2O_3/SiO_2 (In: 3 wt %) was prepared by impregnation of a nitric acid solution of In(acetylacetonate)$_3$ in a pore-filling fashion. The impregnated catalyst was then calcined in the air at 400 °C for 1 h.

Characterization. The crystal structure of prepared intermetallic compounds was examined by powder X-ray diffraction (XRD) with a Rigaku RINT2400 using an X-ray Cu Kα source. Estimation of the crystallite size was performed for the most intense peak, based on the Scherrer equation with a 0.9 Scherrer constant. Transmission electron microscopy (TEM) was conducted on JEOL JEM-2010F at the accelerating voltage of 200 kV. Quantitative elemental analysis of a microscopic region was also performed using energy dispersive X-ray spectroscopy (EDX) equipped with TEM (EDAX, Genesis). In order to prepare the TEM specimen, all samples were sonicated in tetrachloromethane and dispersed on a copper grid supported by an ultrathin carbon film. X-ray photoelectron spectra (XPS) of fresh and spent catalysts were recorded using an ULVAC PHI 5000 VersaProbe spectrometer. Fresh catalysts were pressed into a pellet and placed in a quartz reactor, where it was reduced under flowing hydrogen (60 mL·min^{-1}) at 600 °C for 1 h. Spectra were obtained with an Al Kα X-ray source using C 1s (248.8 eV) for the calibration of binding energy. For spent catalysts, boron nitride (BN, 99%; Wako) was physically mixed into the sample with no reduction pretreatment performed. Energy calibration was conducted with N 1s (398.1 eV) of BN to avoid the contribution of formed coke to the calibration with C 1s. The reduction behavior of the second metal M of Pd_mM_n/SiO_2 was examined by temperature-programmed reduction (TPR). Prior to measurement, the prepared catalyst was calcined at 400 °C for 4 h in air. Under flowing H_2(5%)/Ar, the temperature of the sample bed was raised from room temperature to 800 °C at a heating rate of 10 °C·min^{-1}, and the consumption of hydrogen was continuously measured by a thermal conductivity detector (TCD). The amount of coke formed on the catalysts during the reaction was determined by thermogravimetry (TG) using an SII TG/DTA 7200. The sample (16 mg) was heated from room temperature to 800 °C at a ramping rate of 10 °C·min^{-1}, under a flow of air. The amount of exposed Pd on the catalyst was estimated by CO pulse adsorption. Prior to measurement, the catalyst was reduced under flowing hydrogen (60 mL·min^{-1}) at 400 °C for 0.5 h, followed by He treatment (60 mL·min^{-1}) at 400 °C for 1 h to remove adsorbed hydrogen. After cooling to room temperature, the catalyst bed was cooled to −80 °C (dry ice with acetone). A specific amount of CO(5%)/He pulse was introduced to the catalyst bed and passed (unadsorbed) CO was measured by a TCD. The reduction treatment was omitted for the spent catalyst.

Dehydrogenation of Hydrocarbons. Oxidative dehydrogenation of 1-butene was conducted in a fixed bed flow system with a quartz reactor of 8 mm internal diameter. The dead volume of the reactor was minimized by casting a quartz tube (6 mm outside diameter) to reduce the contribution of hydrocarbon thermal reaction. The catalyst (50 mg) was reduced under flowing hydrogen (99.9999%, 60 mL·min^{-1}; Nippon Sanso) at 400 °C for 1 h prior to the reaction. The reactor was purged with He, followed by feeding of the reaction mixture: 1-butene (>98%, 15 mL·min^{-1}; Takachiho Kogyo), O_2 (15 mL·min^{-1}), and He (90 mL·min^{-1}) at 400 °C. The produced hydrocarbons, including CH_4, were analyzed using a flamed-ionization-detector gas chromatograph (FID−GC, Shimadzu GC-14B) with a column of CP-Silica PLOT (VARIAN, 0.32 mm × 30 m). CO_x (CO and CO_2), O_2, and CH_4 were analyzed using an on line TCD−GC (Shimadzu GC-8A) with a column of active carbon (GL science). CH_4 was analyzed using both FID−GC and TCD−GC to integrate the

dx.doi.org/10.1021/cs500920p | ACS Catal. 2014, 4, 3533−3542

amounts of hydrocarbons and CO_x. Oxidative dehydrogenation of *n*-butane (>99%, Takachiho Kogyo) to 1,3-butadiene was also conducted in a similar fashion, at a reduction and reaction temperature of 500 °C with 30 mg of catalyst. The reaction using $^{18}O_2$ was conducted in a glass circulation system equipped with a vacuum line and a Quadrapole Mass Spectrometer (Spectra International, MICROVISION). Pd/SiO_2 (50 mg) was reduced under flowing hydrogen (60 mL·min^{-1}) at 400 °C for 0.5 h, followed by evacuation. A mixture of 1-butene (1.2 kPa) and $^{18}O_2$ (>99 atom %, 0.46 kPa; ISOTEC) was introduced into the reactor at 400 °C. In the case of $PdIn/SiO_2$ (200 mg), a similar procedure was employed, except that the catalyst was oxidized under 2.0 kPa of $^{18}O_2$ at 400 °C after the reduction treatment. The H_2O/CO_2 molar ratio was determined as a product of the corresponding mass intensity ratio and the correlation coefficient of the calibration curve (0.68).

RESULTS AND DISCUSSION

Figure 1 shows XRD patterns of the prepared catalysts. Pd/SiO_2 displayed two broad peaks assigned to 111 and 200

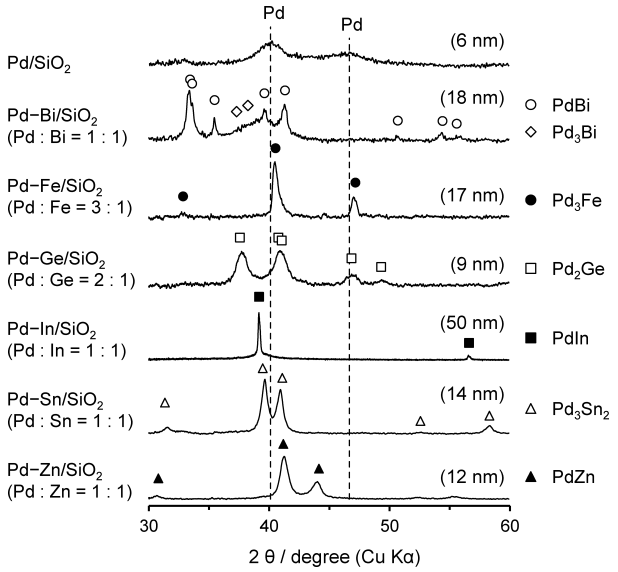

Figure 1. XRD patterns of Pd-based intermetallic compounds supported on silica. Figures in parentheses indicate crystallite size.

diffractions of metallic Pd at 40.1° and 45.2°, respectively. The crystallite size of Pd particles was estimated as 6 nm using Scherrer's equation with the 111 diffraction. The crystallite size was roughly consistent with the particle size (5–9 nm) observed in the TEM image, as shown in Figure 2a. For the Pd–Bi (1:1) catalyst, the desired PdBi intermetallic phase was predominantly observed, indicating the formation of the PdBi phase as the main species. A small broad feature assigned to the Pd_3Bi phase was also observed.[16] The XRD pattern of the Pd–Fe (3:1) catalyst agreed with that of the intermetallic Pd_3Fe phase. The appearance of the 110 diffraction at 33.1° strongly supported the formation of a Pd_3Fe intermetallic phase (space group: *Pm*−3m) but not of a $Pd_{0.75}Fe_{0.25}$ alloy phase (space group: *Fm*−3m). In general, the 110 diffraction of the fcc structure (*Fm*−3m) is not observed by distinction rule due to its high symmetry. For other bimetallic systems, the desired intermetallic compounds (Pd_2Ge, PdIn, Pd_3Sn_2, PdZn) were formed in a single-phase. The estimated crystallite sizes of the

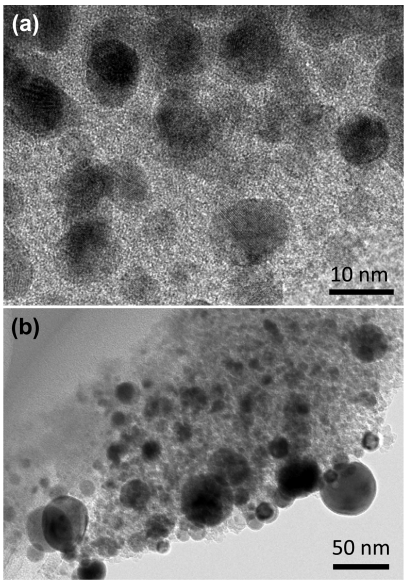

Figure 2. TEM images of (a) Pd/SiO_2 and (b) $PdIn/SiO_2$.

intermetallic compounds were larger than that of monometallic Pd, and differed from each other. No obvious correlation was observed between crystallite size and preparation procedure (successive or coimpregnation), reduction temperature, and Pd/M ratio. Interestingly, PdIn was much larger in size (50 nm) than other intermetallic compounds, despite having with the lowest reduction temperature (400 °C). This may be due to the low melting point of In (157 °C); the lower melting point increases its mobility on the SiO_2 surface and promotes aggregation. In the XRD pattern of PdIn, a broad feature overlapped with the intense sharp peak was observed. Peak deconvolution with two Lorenzian curves well-reproduced the experimental data (Supporting Information, Figure S1). The broader component gave a 5 nm estimation of the crystallite size. The presence of small and large particles was confirmed by TEM, as shown in Figure 2b. The estimated crystallite sizes were consistent with the actual particle size observed in the TEM image.

The catalytic properties of the prepared intermetallic compounds were investigated in the oxidative dehydrogenation of 1-butene to 1,3-butadiene, as shown in Figure 3. In all cases, isomerization into 2-butene and combustion into CO_x also proceeded, as side or main reactions. As anticipated, combustion predominantly proceeded over Pd/SiO_2; therefore, the 1,3-butadiene yield was very low. In contrast, intermetallic catalysts, with the exception of Pd_3Sn_2, showed higher 1,3-butadiene selectivities and yields than Pd/SiO_2, with comparable 1-butene conversion. Pd_3Fe had the highest 1,3-butadiene yield, followed by PdIn and PdBi. The catalytic properties of these catalysts were also tested in the oxidative dehydrogenation of *n*-butane (Figure S2). Dehydrogenation products (1-butene and 1,3-butadiene) were hardly generated over Pd/SiO_2. The selectivity of the combustion products (CO_x: 97 C-%) was higher than in 1-butene dehydrogenation. On the other hand, dehydrogenation occurred to some extent over intermetallic compounds. PdIn showed much higher selectivity to dehydrogenation products (20 C-%) than monometallic Pd (1.8 C-%). Although the selectivity was not sufficiently high, emphasis should be placed on the remarkable increase in selectivity using the intermetallic catalyst. The order

dx.doi.org/10.1021/cs500920p | ACS Catal. 2014, 4, 3533−3542

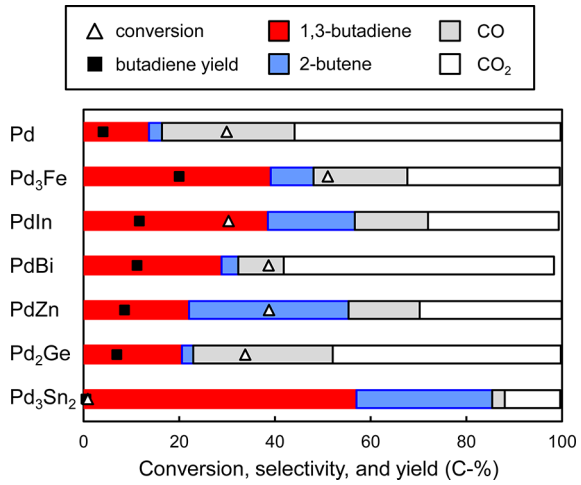

Figure 3. Catalytic performances of Pd-based catalysts in the oxidative dehydrogenation of 1-butene.

of catalytic performances (yield of dehydrogenation products) was similar to that in 1-butene dehydrogenation (1,3-butadiene yield). In both dehydrogenation reactions, conversions of O_2 in the case of most catalysts were ca. 100%.

To understand the mechanism of the remarkable increase in the catalytic performances, we subsequently performed detailed characterizations using $PdIn/SiO_2$ that showed high catalytic performances in both dehydrogenation reactions. Figure 4

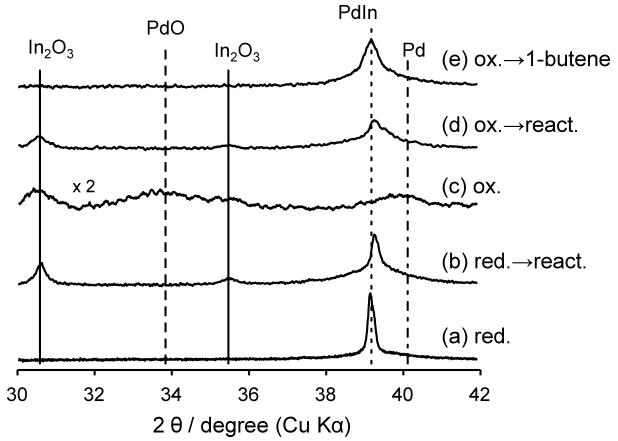

Figure 4. XRD patterns of a $PdIn/SiO_2$ catalyst after treatment at 400 °C with various conditions: (a) H_2 reduction, (b) 1-butene/O_2/He (reaction) after (a), (c) oxidation in the air, (d) 1-butene/O_2/He (reaction) after (c), and (e) 1-butene/He after (c).

shows XRD patterns of $PdIn/SiO_2$ catalyst pretreated under various conditions. PdIn intermetallic phase was solely observed after reduction pretreatment (a). $PdIn/SiO_2$ catalyst spent in oxidative dehydrogenation of 1-butene showed small peaks assigned to In_2O_3 with the 111 diffraction of remaining PdIn (b), indicating some In in PdIn was oxidized by O_2 during the reaction. Formation of In_2O_3 from PdIn should be associated with the formation of Pd. However, no Pd particle, observable by XRD, was detected. Interestingly, the peak position of the 111 diffraction of PdIn was shifted slightly higher in angle. The PdIn (space group: $Pm-3m$) intermetallic phase is classified in the Berthollide-type intermetallic compound, having a small solubility range (e.g., 50−57 Pd atom % for PdIn).[17] Therefore, the peak shift can be attributed to a decrease in the PdIn lattice constant by an increase in Pd/In ratio. These results strongly indicate that the formation of In_2O_3 from PdIn resulted in the formation of $PdIn_{1-\delta}$. The actual composition ratio can be estimated as $Pd_{0.55}In_{0.45}$ (δ = 0.18) by shifting the peak position. It is also likely some Pd formed small monometallic clusters unobservable with XRD. Calcination of $PdIn/SiO_2$ under air caused a disappearance of the PdIn intermetallic phase and a formation of In_2O_3, Pd, and PdO, showing complete decomposition of the PdIn phase (c). The detection of metallic Pd by XRD suggests that the small Pd clusters grew up to be observable with the deep oxidation of PdIn. We also performed oxidative dehydrogenation of 1-butene using the calcined $PdIn/SiO_2$ catalyst. Surprisingly, the spent catalyst showed a similar XRD pattern to (b): peaks assigned to In_2O_3 and $PdIn_{1-\delta}$ were observed (d). This result indicates that a part of In_2O_3 was reduced by 1-butene and PdIn intermetallic phase was regenerated. The reduction of In_2O_3 by 1-butene was confirmed in dehydrogenation of 1-butene without O_2 using the calcined $PdIn/SiO_2$; In_2O_3 completely disappeared and PdIn was regenerated (e). In this case, 1-butene can be regarded as a reducing agent (or hydrogen donor) for In_2O_3, in other words, dehydrogenation of 1-butene is induced by the lattice oxygen of In_2O_3. The pronounced reducibility of In_2O_3 can be found in the literature;[18,19] Penner et al. reported that In_2O_3 was reduced not only by H_2 but even by CO. Based on these results, redox of In and dehydrogenation by lattice oxygen are significantly involved in the catalytic cycle of the Pd−In system.

In this context, it is important to investigate the effect of the oxide species reducibility on catalytic performance. We therefore performed a TPR study using calcined intermetallic catalysts and Pd/SiO_2, as shown in Figure 5. The TPR profile

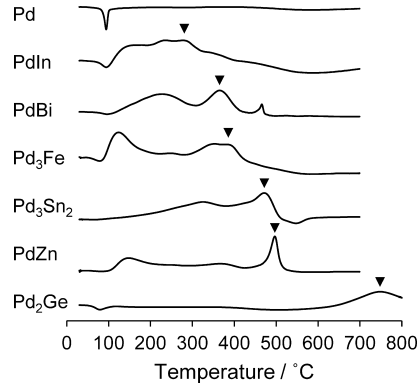

Figure 5. TPR profiles of Pd-based catalysts calcined at 400 °C. Filled triangles indicate the position of the most intense peak assigned to the reduction of the second metal oxide.

of the calcined Pd/SiO_2 did not reveal any positive consumption peak, only a negative peak. It has been reported that PdO is reduced by H_2, even at room temperature.[20−24] Therefore, Pd should be in a metallic state before the temperature becomes elevated. The observation of a negative peak in the TPR profile of Pd is well-known and attributed to the release of H_2 from β-PdH_x species.[20−25] Similar negative peaks were also observed with the calcined intermetallic compounds. In the case of Pd-based bimetallic systems,[21,23,26,27] the formation of PdH_x species tends to be inhibited, relative to monometallic Pd. Therefore, the appearance of the negative peaks supports the decomposition

dx.doi.org/10.1021/cs500920p | ACS Catal. 2014, 4, 3533−3542

of the intermetallic phase into Pd and the second metal oxide. For intermetallic compounds, several reduction peaks were observed. We classified these into two categories: lower (100–250 °C) and higher (>300 °C) temperature. The lower group can be assigned to the reduction of PdO,[21,23,28,29] with a relatively strong interaction with the second metal oxide.[21,29] The higher category is assigned to the second metal oxide.[22,28,29] The reduction temperatures of the lower group were not so different from each other, whereas those of the higher category differed significantly depending on the second metal. Figure 6 shows the relation between the product yield in

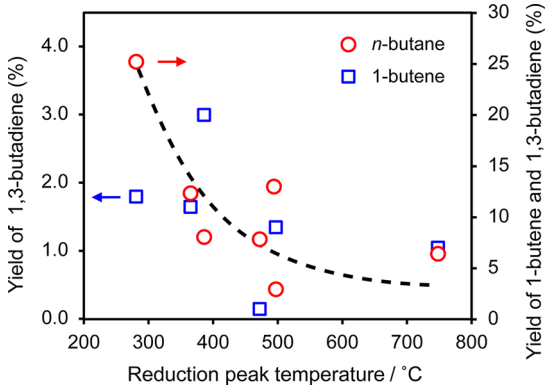

Figure 6. Relation between yield of dehydrogenation products in the oxidative dehydrogenation of 1-butene or *n*-butane over Pd-based intermetallic catalysts and reduction peak temperature of the second metal in TPR profiles.

oxidative dehydrogenation of *n*-butane or 1-butene and the temperature of the most intense reduction peak (filled triangles) of the second metal oxide in TPR profiles. The lower reduction temperature gave a higher product yield in both reactions. These trends were prominent below reduction temperatures of 400 or 500 °C, which was the reaction temperature of the dehydrogenation of 1-butene or *n*-butane, respectively. These results strongly indicate that the reduction of the second metal oxide is the key step for the bimetallic catalysis and, hence, supports involvement of the redox of the second metal.

To understand the interplay of Pd and In in the catalysis, several control experiments were tested using the following catalysts: Pd/SiO_2, $PdIn/SiO_2$, In_2O_3/SiO_2, Pd/In_2O_3, and $Pd/SiO_2 + In_2O_3$ (physical mixture). Figure 7 shows their catalytic performances in the oxidative dehydrogenation of 1-butene. In_2O_3/SiO_2 had much lower conversion and selectivity than Pd/SiO_2 and $PdIn/SiO_2$, suggesting that Pd is necessary to activate the C–H bonds for dehydrogenation. In this case, 2-butene was generated as a main product with almost 1:1 cis/trans ratio (data not shown), indicating that isomerization of 1-butene proceeded over Brønsted acid sites on In_2O_3.[30] Pd/In_2O_3 exhibited higher conversion and selectivity than Pd/SiO_2 and a comparable 1,3-butadiene yield to that of $PdIn/SiO_2$. This result suggests that a combination of Pd and In_2O_3 is important to obtained high catalytic performance. Physical mixture of Pd/SiO_2 and bulk In_2O_3, however, did not enhance selectivity compared to Pd/SiO_2. On the basis of these results, we concluded that a key point for selective dehydrogenation is that Pd and In_2O_3 are adjacent in the atomic order.

To discuss the nature of the reaction site and mechanism in detail, multiple characterization of the catalyst structure is

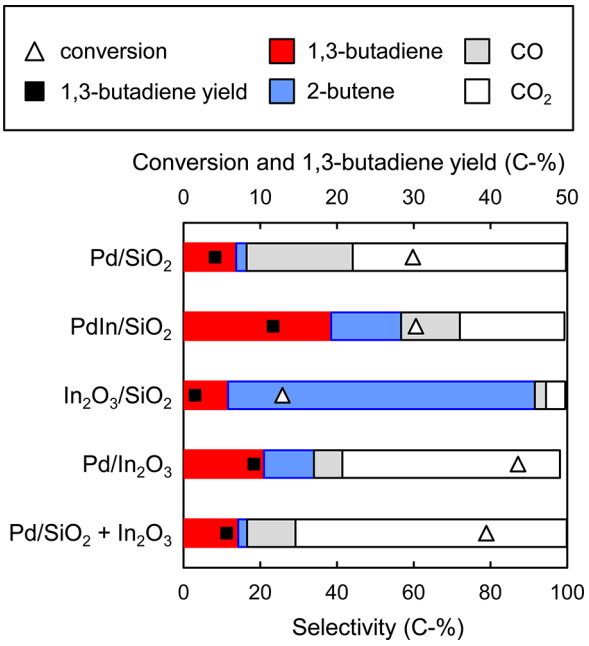

Figure 7. Catalytic performances in 1-butene dehydrogenation over various In_2O_3-containing materials.

required. Therefore, we conducted FT-IR, XPS and TEM–EDX analyses on the $PdIn/SiO_2$ catalysts spent in oxidative dehydrogenation of 1-butene. Figure 8 shows the FT-IR spectra

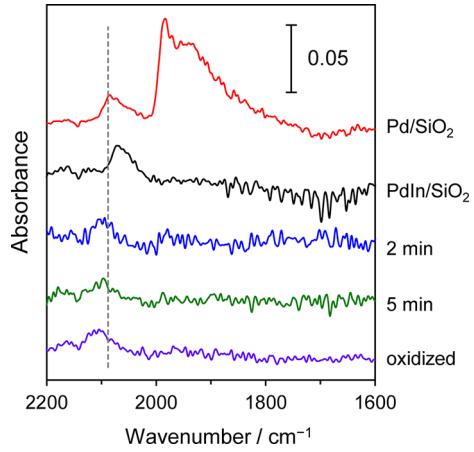

Figure 8. FT-IR spectra of CO adsorbed on fresh Pd/SiO2 and $PdIn/SiO_2$. Data for $PdIn/SiO_2$ spent in oxidative dehydrogenation of 1-butene (for 2 and 5 min) and oxidized by O_2 at 400 °C for 1 h were also shown.

of CO adsorbed on fresh and spent catalysts. CO adsorbed on fresh Pd/SiO_2 exhibited peaks assigned to linearly adsorbed CO on Pd at 2088 cm^{-1} and bridged CO at around 1950 cm^{-1}.[31] For fresh $PdIn/SiO_2$, no bridged species were observed, which corresponds to the disappearance of Pd ensembles by the formation of the intermetallic compound. The peak position of linear CO on $PdIn/SiO_2$ was lower in energy than that on Pd/SiO_2 (2065 cm^{-1}), indicating that Pd atoms in PdIn were negatively charged compared with those in monometallic Pd. This result is consistent with a similar previously reported FT-IR study.[32] After the reaction, however, the peak position shifted to that of Pd/SiO_2. This position was very close to that of $PdIn/SiO_2$ oxidized by O_2, which decomposed into Pd and

dx.doi.org/10.1021/cs500920p | ACS Catal. 2014, 4, 3533–3542

In_2O_3. These results support the formation of monometallic Pd at the catalyst surface under the reaction condition. Moreover, the absence of bridged CO on the spent $PdIn/SiO_2$ indicates that the generated Pd was highly dispersed or isolated. The slight deviation of the peak position between pure Pd/SiO_2 and the spent or oxidized $PdIn/SiO_2$ may be due to a difference in the surrounding species of Pd, either SiO_2 or In_2O_3. Figure 9

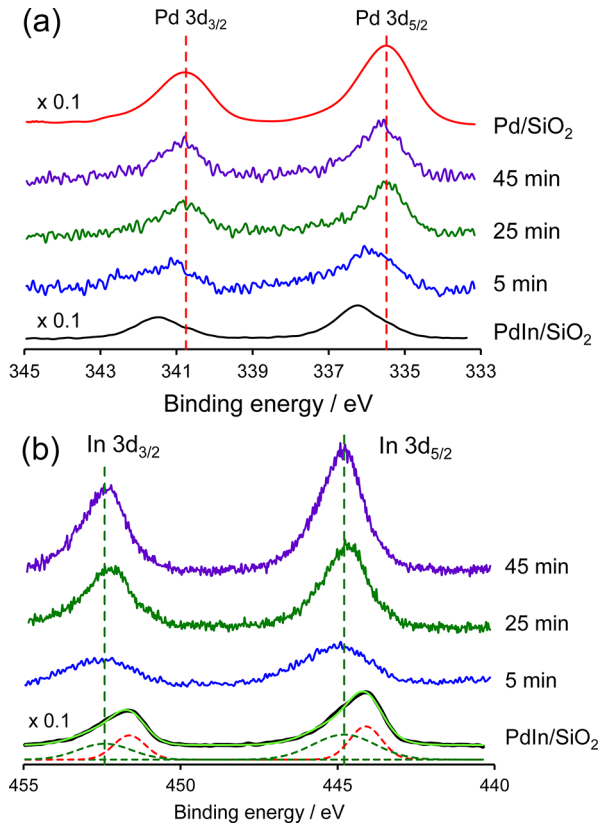

Figure 9. (a) Pd 3d and (b) In 3d XPS of $PdIn/SiO_2$ before and after oxidative dehydrogenation of 1-butene.

shows (a) Pd 3d and (b) In 3d XPS for fresh and the spent catalysts. Pd/SiO_2 indicated $3d_{5/2}$ and $3d_{3/2}$ emissions at 335.5 and 340.8 eV, respectively, consistent with the reported values of metallic Pd supported on SiO_2.[33] The peak positions of Pd $3d_{5/2}$ and $3d_{3/2}$ for the fresh $PdIn/SiO_2$ (336.3 eV for $3d_{5/2}$ and 341.5 eV for $3d_{3/2}$) were higher in energy than those of monometallic Pd/SiO_2. The higher binding energy with $PdIn/SiO_2$ is seemingly contradictory to the negatively charged Pd as mentioned in the FT-IR study. Similar results have also been reported for PdGa[27,34] and PdZn.[35−37] In these cases, valence band XPS and DFT calculations revealed that the valence band of the intermetallic compound was occupied to a higher degree than that of monometallic Pd, making Pd atoms negatively charged.[27,34] The higher binding energy in the Pd 3d core level was interpreted as a change in the screening of the core holes by the increased occupancy of the valence band.[37] As the reaction proceeded, the peak feature gradually changed into that of the monometallic Pd. After 25 min, the peaks agreed well with that of Pd/SiO_2. The In 3d XPS of flesh $PdIn/SiO_2$ are deconvoluted into two components: metallic In in PdIn (444.1 and 451.6 eV)[38] and In^{3+} (444.8 and 452.4 eV).[38,39] The presence of the In^{3+} species in fresh $PdIn/SiO_2$ indicates that a small fraction of In did not participate in the formation of the PdIn phase and remained as In_2O_3. The presence of a small amount of In_2O_3 corresponds to a slight surplus of Pd species due to the 1:1 Pd:In loading ratio. Indeed, a trace amount of monometallic Pd was observed in the Pd 3d XPS as a small shoulder. The composition of In_2O_3 increased, reaching almost 100% as the reaction proceeded. These results support the decomposition of PdIn into Pd and In_2O_3. Although $PdIn_{1-\delta}$ was mainly observed by XRD, the XPS results did not indicate the presence of intermetallic Pd species at the catalyst surface after 25 min. According to these results, a core−shell structure, in which the $PdIn_{1-\delta}$ core is covered with a In_2O_3 shell containing Pd clusters, is likely to be formed in the reaction. This is consistent with PdIn being oxidized by O_2 from outside of the particle. Comparing the results of FT-IR and XPS, the change in the catalyst structure observed in the FT-IR study completed at a much earlier stage (5 min) than that in the XPS study (25 min). This deviation can be attributed to the fact that XPS includes information about the near-surface region, whereas FT-IR study using CO as a probe molecule only provides the information on the outmost layer. These are also consistent with the oxidation of PdIn from the outside. Figure 10 shows TEM images of nanoparticles on the fresh and the

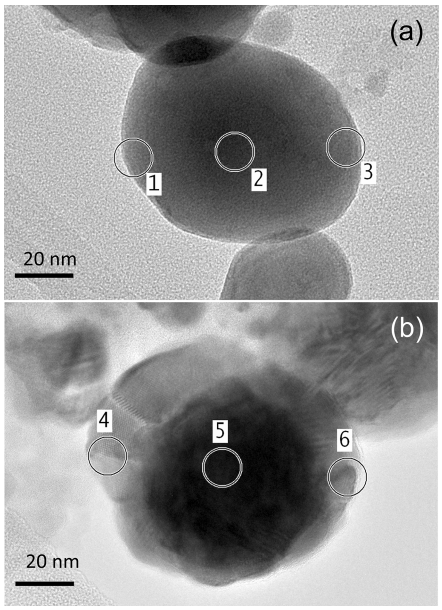

Figure 10. TEM images of $PdIn/SiO_2$ catalyst: (a) fresh and (b) spent in the dehydrogenation of 1-butene. Circles indicate where EDX analysis was performed.

spent $PdIn/SiO_2$ catalysts. Chemical analyses by EDX were also conducted at the edge and center of the nanoparticles (Nos. 1−6 designated with circles). The atomic ratio of Pd, In, and O at each point is listed in Table 1. Fresh catalyst had Pd/In ratios close to 1:1, regardless of the position (Nos. 1−3), supporting homogeneous formation of the PdIn intermetallic compound. However, In contents were slightly lower than Pd, with the differences close to O content. This is consistent with the observation of In_2O_3 at the catalyst surface by XPS. After the reaction, the structure of the nanoparticle drastically changed, as shown Figure 9b; the particle indeed had a core−shell structure consisting of a dark core and relatively bright shell. The EDX analysis on the particle center (No. 5) revealed a composition ratio with high Pd content: Pd (55) > In (28) > O (17). Assuming that Pd atoms form $Pd_{0.55}In_{0.45}$ and

dx.doi.org/10.1021/cs500920p | ACS Catal. 2014, 4, 3533−3542

Table 1. EDX Analysis of Atomic Composition of Fresh and Spent $PdIn/SiO_2$ Catalysts

		atomic composition (%)[b]		
catalyst	site no.[a]	Pd	In	O
fresh	1	50.7(2)	43.7(3)	6.3(13)
	2	48.2(5)	42.2(8)	9.6(32)
	3	47.3(1)	42.5(2)	10.2(7)
spent	4	20.3(1)	50.6(1)	29.3(1)
	5	54.8(2)	27.7(4)	17.5(9)
	6	38.2(5)	31.5(8)	30.3(14)

[a]Site numbers correspond to those designated in Figure 9. [b]Figure in parentheses indicates an error in the first decimal place.

monometallic Pd, we can estimate the composition ratio of $Pd/Pd_{0.55}In_{0.45}/In_2O_3$ as 6.1:3.6:1.0. A considerable amount of Pd seems to be in the monometallic phase, consistent with XPS results. On the other hand, the edge regions were mainly composed of In and O (Nos. 4 and 6). Therefore, formation of a core−shell structure consisting of the $PdIn_{1-\delta}$ core and the $Pd-In_2O_3$ shell was demonstrated. The relatively high Pd content at the center can be attributed to the presence of noncrystalline Pd clusters at the surface or near-surface region. Because EDX analysis is performed by acquiring transmitted X-rays along with the zone axis of the observation, a small contribution of the near surface region should be included in the output. Based on the Pd content comparable with the In content at the shell (No. 6) and the substantial width of the shell, the observed high Pd content at the center (No. 5) is compatible with the core−shell structure. Figure S3 shows a high-resolution TEM image of the core−shell particle. At the shell region, lattice fringes (4.12 Å) corresponding to In_2O_3 (211) planes (4.13 Å) were clearly observed. In contrast, at the core region, lattice fringes with 2.32 Å were observed overlapped with those of In_2O_3, which is consistent with the *d* spacing of PdIn (110) planes (2.30 Å). However, this spacing is also similar to that of Pd (111) (2.25 Å). Considering a few percent error, an additional support is required for assignment to the PdIn phase. In this context, the fact that the core is composed of a large crystallite reinforces the assignment, as the presence of crystalline PdIn has been demonstrated by XRD analysis.

Scheme 1a illustrates the change in the catalyst structure during the reaction. In atoms of PdIn are oxidized into In_2O_3 from the surface by O_2. Generation of In_2O_3 from PdIn forms small monometallic Pd clusters that are unobservable by XRD. The remaining intermetallic phase core is covered with a In_2O_3 layer shell containing small Pd clusters and the In content of the core is decreased slightly by the transformation to $PdIn_{1-\delta}$. According to the results observed above, a similar structure was formed under dehydrogenation of 1-butene regardless of whether the reduced or calcined catalyst was used, and the catalyst seemed to reach a steady-state structure. In this case, both catalysts showed comparable 1,3-butadiene yields even after 5 min of TOS (Table S1). This is consistent with the result of the FT-IR study that the catalyst structure at the surface reaches the steady-state at the initial stage of the reaction.

On this experimental basis, we proposed the following reaction mechanism for the oxidative dehydrogenation of hydrocarbons over $PdIn/SiO_2$ (Scheme 1b). Initially, surface PdIn is oxidized into Pd and In_2O_3 (1). Pd and In_2O_3 are placed adjacent to each other during this process. Oxidative

Scheme 1. (a) Change in Catalyst Structure during the Reaction and (b) Proposed Reaction Mechanism of the Oxidative Dehydrogenation of 1-Butene to 1,3-Butadiene over $PdIn/SiO_2$[a]

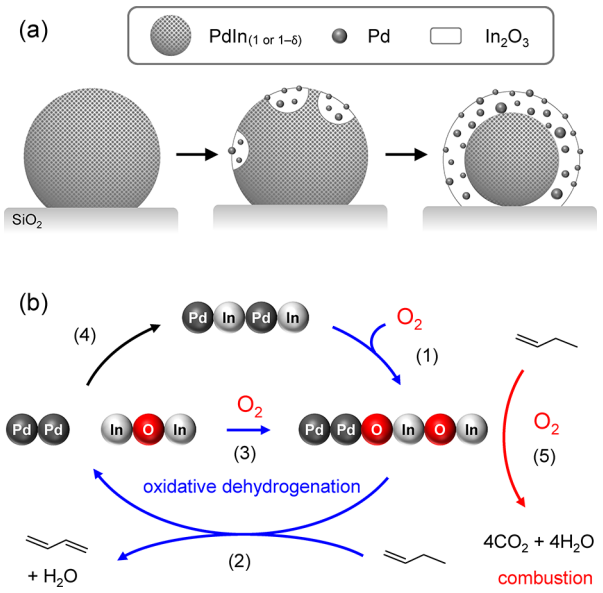

[a]Reaction mechanism: (1) oxidative decomposition of PdIn to Pd and In_2O_3, (2) dehydrogenation of 1-butene to 1,3-butadiene at the interface, (3) reoxidation of In by O_2, (4) over-reduction, and (5) combustion by O_2.

dehydrogenation of the hydrocarbon occurs at the interface through C−H activation via Pd and hydrogen consumption by the lattice oxygen of In_2O_3 to form water (2). This step can be regarded as partial reduction of In_2O_3 by the hydrocarbon. The oxygen vacancy is filled by reoxidation with O_2 (3). Over-reduction of In_2O_3 to metallic In may regenerate the parent PdIn phase (4). O_2 is also used for combustion of hydrocarbon over Pd sites (6). Therefore, the selectivity for dehydrogenation strongly depends on whether O_2 is taken to form lattice oxygen of In_2O_3 or is directly used for combustion. In other words, incorporation of O_2 into the lattice of In_2O_3 decreases its opportunity to be used in combustion. In the case of the Pd/In_2O_3 catalyst, a similar chemical process may occur at the interface of Pd particles and In_2O_3 supports. Indeed, it has been reported that a PdIn phase is formed by reduction treatment with Pd/In_2O_3 and that the subsequent oxidation treatment causes decomposition of the PdIn phase to Pd and In_2O_3.[40] However, one should consider the ratio of $Pd-In_2O_3$ interfacial sites and monometallic Pd sites, which has a determining influence on selectivity for dehydrogenation. In the case of PdIn, the adjacency of Pd and In, on an atomic scale, provides highly dispersed Pd sites and maximizes the number of $Pd-In_2O_3$ sites. In contrast, in the case of Pd/In_2O_3, the corresponding process can occur only at the interfacial site. This difference may be the reason for the 2-fold deviation in selectivity.

To confirm that the $Pd-In_2O_3$ composite indeed shows a higher selectivity to oxidative dehydrogenation than Pd, we evaluated H_2O/CO_2 ratios in the reactions (Scheme 2). For example, oxidative dehydrogenation of one 1-butene molecule yields equimolar amounts of 1,3-butadiene and H_2O, whereas combustion of 1-butene gives 4 CO_2 and 4 H_2O (Scheme 2a). Therefore, the H_2O/CO_2 ratio reflects the selectivity to

dx.doi.org/10.1021/cs500920p | ACS Catal. 2014, 4, 3533−3542

Scheme 2. (a) Products in the Oxidative Dehydrogenation and Combustion of 1-Butene and $[H_2{}^{18}O]/[C^{18}O_2]$ Ratios Obtained in the Presence of (b) 1-Butene, $^{18}O_2$, and Pd/SiO_2 and (c) 1-Butene and Pd–$In_2{}^{18}O_3/SiO_2$

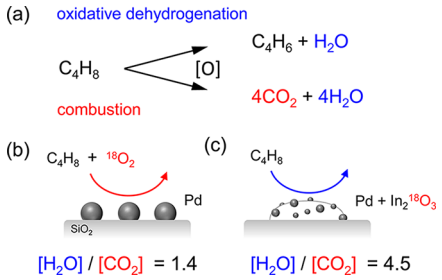

dehydrogenation or combustion. To evaluate the ratio in the reaction with O_2 in the absence of In_2O_3, 1-butene and $^{18}O_2$ were introduced on Pd/SiO_2 at 400 °C. $^{18}O_2$ was used to distinguish CO_2 ($C^{16}O_2$, MW: 44) from C_3H_8 (MW: 44), fragmented from C_4H_8. The ratio, 1.4, was close to unity (Scheme 2b), indicating that combustion was dominant. On the other hand, the reaction over Pd–$In_2{}^{18}O_3$ composite ($PdIn/SiO_2$ calcined under $^{18}O_2$) gave a much higher H_2O/CO_2 ratio (4.5, Scheme 2c). These results demonstrated that combustion was indeed suppressed in the presence of In_2O_3.

We subsequently performed a kinetic study in oxidative dehydrogenation of 1-butene over Pd/SiO_2 and $PdIn/SiO_2$.[41] The dependences of the formation rate of 1,3-butadiene on partial pressure of 1-butene ($P_{C_4H_8}$) and O_2 (P_{O_2}) were as follows (eqs 3 and 4):

$$r_{C_4H_6} = kP_{C_4H_8}{}^{0.97}P_{O_2}{}^{0.38}\ (Pd/SiO_2) \quad (3)$$

$$r_{C_4H_6} = kP_{C_4H_8}{}^{0.17}P_{O_2}{}^{1.04}\ (PdIn/SiO_2) \quad (4)$$

For Pd/SiO_2, a first-order relationship with P_{C4H8} was observed, whereas the dependence on P_{O2} was low. This result suggests that adsorption of 1-butene on Pd surface is the rate-determining step and the catalyst surface was dominantly covered with O_2. The excess amount of O_2 on the catalyst surface compared to 1-butene seems to easily result in undesired combustion. This is also consistent with the results observed in Figure 3. On the other hand, $PdIn/SiO_2$ exhibited opposite features (i.e., a first-order relationship with P_{O2} and almost zero-order dependence on P_{C4H8}). Hence, 1-butene saturated the catalyst surface, and adsorption of O_2 (or oxidation of In to In_2O_3) was the rate-determining step for $PdIn/SiO_2$—a situation favorable for the dehydrogenation process, in preference to combustion.

Finally, the stability of the catalyst during the oxidative dehydrogenation of 1-butene was tested. Figure 11 (red circles) shows the time course of 1,3-butadiene yield during the reaction. The product yield decreased slightly with time on stream, almost plateauing around 135 min. The amount of coke deposited on the catalyst, determined by TG-DTA analysis (see Supporting Information Figure S4 for the results of TG-DTA), was also plotted versus time on stream (Figure 10, black diamonds). The amount of coke increased at the initial stage of the reaction, becoming saturated around 135 min.[42] A negative linear correlation was observed between butadiene yield and the amount of coke (Figure 10, blue triangles), suggesting a diminished catalytic performance attributable to a decrease in the number of active sites due to coke deposition. Although a

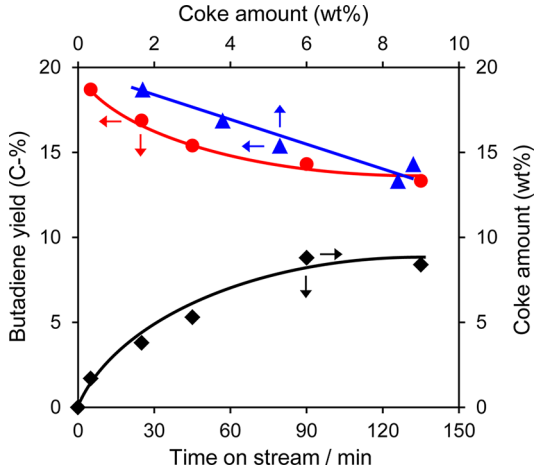

Figure 11. Time course of 1,3-butadiene yield (red circles) and coke amount (black diamonds) in oxidative dehydrogenation of 1-butene over $PdIn/SiO_2$ and the relation between them (blue triangles).

slight deactivation occurred, it should be noted that this catalytic system possesses resistance to coke accumulation. The saturation of coke amount during the reaction is probably due to a steady state being reached between coke formation and combustion. We also measured the change in the amount of exposed Pd by CO adsorption among the spent catalysts (Figure S5). The amount of exposed Pd was halved in the initial stage of the reaction (~5 min), followed by a moderate decline (5–135 min). The initial drop corresponds to the change in the catalyst surface structure from PdIn to a Pd–In_2O_3 composite. The latter decrease can be attributed to coke deposition. In contrast, turnover frequency did not so vary during the reaction (5–90 min). These results support that the decrease in 1,3-butadiene yield is due to coke deposition.

On the basis of the insights obtained in this study, the unique catalytic property of the Pd-based intermetallic compounds observed in this study appears to correlate with the reducibility of the second metal element. As mentioned above, the high reducibility of In_2O_3 may contribute to the catalytic property. In addition to the reducibility, the formation enthalpy (ΔH_f) of the intermetallic compound (i.e., the easiness of compound formation) may be involved. In general, the more negative ΔH_f, the more negative the corresponding ΔG_f, promoting compound formation. For example, PdBi has a moderately negative ΔH_f (−27 $kJmol^{-1}$),[43] whereas PdIn has a considerably negative ΔH_f (−61 $kJmol^{-1}$).[44] Moreover, PdIn possesses a certain solubility range, which would make the transferring of In atoms less constrained. Thus, the combination of these specific properties of PdIn may induce the greatest catalytic performance. However, there is still room to improve the selectivity of this catalytic system. Based on the obtained insights, it is important that Pd atoms are highly dispersed or isolated by In_2O_3 during the reaction. Therefore, it is a promising way to reduce the Pd/In ratio below 1 so that Pd atoms become less aggregated. Alternatively, modification of the catalyst support may be an effective way to inhibit aggregation of Pd and/or In_2O_3. Because SiO_2 has a relatively weak metal–support interaction,[45] the loaded species tend to aggregate easily. It is better to employ an appropriate support having a substantially strong metal–support interaction, such as γ-Al_2O_3,[45] so that Pd and In_2O_3 remain well dispersed. In this catalytic cycle, involvement of O_2 is essential for the formation

dx.doi.org/10.1021/cs500920p | ACS Catal. 2014, 4, 3533–3542

of ideal reaction sites. Therefore, a similar catalytic cycle may work in some other reaction systems involving O_2, such as alcohol oxidation, oxidative steam reforming of methanol, and ammonia-deNO_x.

CONCLUSION

In this study, catalytic performances of Pd-based intermetallic compounds (Pd_mM_n/SiO_2: M = Bi, Fe, Ge, In, Sn, Zn) in the oxidative dehydrogenation of 1-butene and *n*-butane were investigated. A remarkable increase in selectivity (and also yield) to dehydrogenation products (1,3-butadiene and/or 1-butene) was obtained when monometallic Pd was replaced by PdIn, PdBi, or Pd_3Fe. Undesired combustion into CO_x proceeded over monometallic Pd, significantly decreasing selectivity. The presence of the second metal (In, Bi, or Fe) adjacent to Pd effectively inhibits undesired combustion, likely by capturing O_2 as a lattice oxygen. The incorporated lattice oxygen reacts with hydrogen atoms derived from the hydrocarbon by C−H activation over Pd sites, resulting in the formation of water and oxygen vacancy and/or the parent intermetallic phase. Thus, a combination of C−H activation by Pd and redox of the second metal provides a unique and effective dehydrogenation process, compared to monometallic Pd or the second metal oxide alone. Under the reaction conditions tested, the catalyst surface decomposes into Pd and the second metal oxide (Pd−MO_x nanocomposite), forming a core−shell structure with a parent intermetallic core and a composite shell as a steady state. The insights obtained in this study will open the way to the development of a more effective dehydrogenation system based on bifunctional catalysis.

ASSOCIATED CONTENT

Supporting Information

Additional catalytic data, peak deconvolution of XRD pattern, TG−DTA, amount of exposed Pd. This material is available free of charge via the Internet at http://pubs.acs.org.

AUTHOR INFORMATION

Corresponding Author

*E-mail: komatsu.t.ad@m.titech.ac.jp. Fax: +81-3-5734-2758. Tel.: +81-3-5734-3532.

Notes

The authors declare no competing financial interest.

ACKNOWLEDGMENTS

This work was supported by JSPS KAKENHI Grant No. 23360353. We thank Center for Advanced Materials Analysis Tokyo Institute of Technology for the aid of TEM−EDX analysis.

REFERENCES

(1) Passmann, W. *Ind. Eng. Chem.* **1970**, *62*, 48−51.
(2) Dumez, F. J.; Froment, G. F. *Ind. Eng. Chem. Proc. Dd* **1976**, *15*, 291−301.
(3) Håkonsen, S. F.; Holmen, A. In *Handbook of Heterogeneous Catalysis*; Ertl, G., Knozinger, H., Schuth, F., Weitkamp, J., Eds.; Wiley-VCH Verlag GmbH & Co. KGaA: Weinheim, 2008; Chapter 14; pp 3384−3386.
(4) Park, J. H.; Noh, H.; Park, J. W.; Row, K. H.; Jung, K. D.; Shin, C. H. *Res. Chem. Intermed.* **2011**, *37*, 1125−1134.
(5) Jung, J. C.; Lee, H.; Kim, H.; Chung, Y. M.; Kim, T. J.; Lee, S. J.; Oh, S. H.; Kim, Y. S.; Song, I. K. *J. Mol. Catal. A: Chem.* **2007**, *271*, 261−265.
(6) Soares, A. P. V.; Dimitrov, L. D.; de Oliveira, M. C. R. A.; Hilaire, L.; Portela, M. F.; Grasselli, R. K. *Appl. Catal., A* **2003**, *253*, 191−200.
(7) Batist, Ph. A.; van de Moesdijk, C. G. M.; Matsuura, I.; Schuit, G. C. A. *J. Catal.* **1971**, *20*, 40−57.
(8) Krishnan, V. V.; Suib, S. L. *J. Catal.* **1999**, *184*, 305−315.
(9) Liaw, B. J.; Cheng, D. S.; Yang, B. L. *J. Catal.* **1989**, *118*, 312−326.
(10) Herniman, H. J.; Pyke, D. R.; Reid, R. *J. Catal.* **1979**, *58*, 68−73.
(11) Gibson, M. A.; Hightower, J. W. *J. Catal.* **1976**, *41*, 420−430.
(12) She, Y.; Han, J.; Ma, Y. H. *Catal. Today* **2001**, *67*, 43−53.
(13) Fujimoto, K.; Kunugi, T. *Ind. Eng. Chem. Prod. Rd.* **1981**, *20*, 319−323.
(14) Onda, A.; Komatsu, T.; Yashima, T. *J. Catal.* **2004**, *221*, 378−385.
(15) Furukawa, S.; Tamura, A.; Ozawa, K.; Komatsu, T. *Appl. Catal., A* **2014**, *469*, 300−305.
(16) Under the reaction atmosphere, any intermetallic species at the catalyst surface will be oxidized into Pd metal and the second metal oxide phases. Therefore, the presence of a small amount of the impurity phase does not seem to strongly affect the reaction outcome.
(17) Okamoto, H. *Desk Handbook: Phase Diagrams for Binary Alloys*; ASM International: Materials Park, OH, 2000.
(18) Bielz, T.; Lorenz, H.; Amann, P.; Klotzer, B.; Penner, S. *J. Phys. Chem. C* **2011**, *115*, 6622−6628.
(19) Bielz, T.; Lorenz, H.; Jochum, W.; Kaindl, R.; Klauser, F.; Klotzer, B.; Penner, S. *J. Phys. Chem. C* **2010**, *114*, 9022−9029.
(20) Bond, G. C.; Tripathi, J. B. P. *J. Chem. Soc., Faraday Trans. 1* **1976**, *72*, 933−941.
(21) Benedetti, A.; Fagherazzi, G.; Pinna, F.; Rampazzo, G.; Selva, M.; Strukul, G. *Catal. Lett.* **1991**, *10*, 215−223.
(22) Iwasa, N.; Mayanagi, T.; Ogawa, N.; Sakata, K.; Takezawa, N. *Catal. Lett.* **1998**, *54*, 119−123.
(23) Batista, J.; Pintar, A.; Mandrino, D.; Jenko, M.; Martin, V. *Appl. Catal., A* **2001**, *206*, 113−124.
(24) Hong, C. T.; Yeh, C. T.; Yu, F. H. *Appl. Catal.* **1989**, *48*, 385−396.
(25) Fagherazzi, G.; Benedetti, A.; Polizzi, S.; Dimario, A.; Pinna, F.; Signoretto, M. *Catal. Lett.* **1995**, *32*, 293−303.
(26) Ziemecki, S. B.; Michel, J. B.; Jones, G. A. *React. Solid* **1986**, *2*, 187−202.
(27) Kovnir, K.; Armbruster, M.; Teschner, D.; Venkov, T. V.; Szentmiklosi, L.; Jentoft, F. C.; Knop-Gericke, A.; Grin, Y.; Schlogl, R. *Surf. Sci.* **2009**, *603*, 1784−1792.
(28) Iwasa, N.; Ogawa, N.; Masuda, S.; Takezawa, N. *Bull. Chem. Soc. Jpn.* **1998**, *71*, 1451−1455.
(29) Pinna, F.; Selva, M.; Signoretto, M.; Strukul, G.; Boccuzzi, F.; Benedetti, A.; Canton, P.; Fagherazzi, G. *J. Catal.* **1994**, *150*, 356−367.
(30) Dapaah, J. K. A.; Uemichi, Y.; Ayame, A.; Matsuhashi, H.; Sugioka, M. *Appl. Catal., A* **1999**, *187*, 107−113.
(31) Kim, W. J.; Shin, E. W.; Kang, J. H.; Moon, S. H. *Appl. Catal., A* **2003**, *251*, 305−313.
(32) Hirano, T.; Kazahaya, Y.; Nakamura, A.; Miyao, T.; Naito, S. *Catal. Lett.* **2007**, *117*, 73−78.
(33) Huang, L.; Wang, Z.; Ang, T. P.; Tan, J.; Wong, P. K. *Catal. Lett.* **2006**, *112*, 219−225.
(34) Kovnir, K.; Armbruster, M.; Teschner, D.; Venkov, T. V.; Jentoft, F. C.; Knop-Gericke, A.; Grin, Y.; Schlogl, R. *Sci. Technol. Adv. Mater.* **2007**, *8*, 420−427.
(35) Armbruster, M.; Behrens, M.; Fottinger, K.; Friedrich, M.; Gaudry, E.; Matam, S. K.; Sharma, H. R. *Catal. Rev.* **2013**, *55*, 289−367.
(36) Iwasa, N.; Takezawa, N. *Top. Catal.* **2003**, *22*, 215−224.
(37) Friedrich, M.; Teschner, D.; Knop-Gericke, A.; Armbruster, M. *J. Catal.* **2012**, *285*, 41−47.
(38) Marchesini, F. A.; Irusta, S.; Querini, C.; Miro, E. *Appl. Catal., A* **2008**, *348*, 60−70.
(39) Skala, T.; Veltruska, K.; Moroseac, M.; Matolinova, I.; Korotchenkov, G.; Matolin, V. *Appl. Surf. Sci.* **2003**, *205*, 196−205.

(40) Lorenz, H.; Turner, S.; Lebedev, O. I.; Van Tendeloo, G.; Klotzer, B.; Rameshan, C.; Pfaller, K.; Penner, S. *Appl. Catal., A* **2010**, *374*, 180−188.
(41) Sampling for the kinetic study was performed at 5 min of TOS, in which time activity already reached a steady state as mentioned above. Therefore, the initial change in the catalytic structure was excluded from the kinetic study.
(42) As the coke amount (e.g., 0.35 mmol at 135 min) corresponds to only 0.1% of the integrated reactant flow (330 mmol for 135 min), its contribution to the carbon balance can be ignored.
(43) Vrest'al, J.; Pinkas, J.; Watson, A.; Scott, A.; Houserova, J.; Kroupa, A. *CALPHAD: Comput. Coupling Phase Diagrams Thermochem.* **2006**, *30*, 14−17.
(44) Jordan, J. L.; Deevi, S. C. *Intermetallics* **2003**, *11*, 507−528.
(45) Furukawa, S.; Ozawa, K.; Komatsu, T. *RSC Adv.* **2013**, *3*, 23269−23277.